

# Radiative data for highly excited $3d^84d$ levels in Ni II from laboratory measurements and atomic calculations

H. Hartman<sup>1,2</sup>, L. Engström<sup>3</sup>, H. Lundberg<sup>3</sup>, H. Nilsson<sup>2,3</sup>, P. Quinet<sup>4,5</sup>, V. Fivet<sup>4</sup>, P. Palmeri<sup>4</sup>, G. Malcheva<sup>6</sup> and K. Blagoev<sup>6</sup>

<sup>1</sup> Material Sciences and Applied Mathematics, Malmö University, 20506 Malmö, Sweden

<sup>2</sup> Lund Observatory, Lund University, Box 43, SE-221 00 Lund, Sweden

<sup>3</sup> Department of Physics, Lund University, Box 118, SE-221 00 Lund, Sweden

<sup>4</sup> Physique Atomique et Astrophysique, Université de Mons, B-7000 Mons, Belgium

<sup>5</sup> IPNAS, Université de Liège, B-4000 Liège, Belgium

<sup>6</sup> Institute of Solid State Physics, Bulgarian Academy of Sciences, 72 Tzarigradsko Chaussee, BG-1784 Sofia, Bulgaria  
e-mail: Henrik.Hartman@mah.se

Received ??; accepted ??

## ABSTRACT

**Aims.** This work reports new experimental radiative lifetimes and calculated oscillator strengths for transitions from  $3d^84d$  levels of astrophysical interest in singly ionized nickel.

**Methods.** Radiative lifetimes of seven high-lying levels of even parity in Ni II (98400 – 100600  $\text{cm}^{-1}$ ) have been measured using the time-resolved laser-induced fluorescence method. Two-step photon excitation of ions produced by laser ablation has been utilized to populate the levels. Theoretical calculations of the radiative lifetimes of the measured levels and transition probabilities from these levels are reported. The calculations have been performed using a pseudo-relativistic Hartree-Fock method, taking into account core polarization effects.

**Results.** A new set of transition probabilities and oscillator strengths has been deduced for 477 Ni II transitions of astrophysical interest in the spectral range 194 – 520 nm depopulating even parity  $3d^84d$  levels. The new calculated gf-values are, on the average, about 20 % higher than a previous calculation by Kurucz (<http://kurucz.harvard.edu>) and yield lifetimes within 5 % of the experimental values.

**Key words.** atomic data – methods: laboratory: atomic – techniques: spectroscopic

## 1. Introduction

The final stage of exothermal element production in massive stars is the iron-group elements, with nickel itself having the maximum binding energy per nucleon closely followed by iron. Higher  $Z$  elements are produced by subsequent neutron capture. Nickel is therefore one of the most abundant iron-peak elements in cosmic objects. In addition, Nickel shows a line-rich spectrum due to its complex atomic structure and the lines appear in a variety of objects, from the interstellar medium and stars to the solar corona and supernova explosions. Nuclear statistical equilibrium models predict that iron and nickel are produced in high-temperature environments, i.e. explosive nucleosynthesis (Nadyozhin 2003), such as supernovae type Ia, where a white dwarf ignites, or supernovae type II, where the core of a massive star collapses into a neutron star (Stritzinger et al. 2006). The dominating product of these events is  $^{56}\text{Ni}$ , which is distributed to the surrounding gas during the outburst. Abundance determinations of nickel in stars serve as important constraints of stellar evolution and supernova explosion models. The current challenges for accurate elemental abundances are the development of 3D-model atmospheres and non-LTE modeling (Wongwathanarat et al. 2011; Lind et al. 2012). Atomic data for levels of different excitation energies are important for this development. For example, in metal-rich stellar photospheres, transitions from low excitation states with a high population can be

saturated whereas those from the less populated highly excited states are more likely to be optically thin. The present investigation of Ni II is part of an ongoing effort to provide such data for the second spectra of selected iron-group elements: Ti II (Lundberg et al. 2016), Cr II (Engström et al. 2014), Fe II (Hartman et al. 2015) and Co II (Quinet et al. 2016).

There are two papers in the literature on experimental determination of radiative lifetimes in Ni II. Lawler & Salih (1987) used the Time-Resolved Laser-Induced Fluorescence (TR-LIF) method on a slow  $\text{Ni}^+$  beam from a hollow-cathode source. Radiative lifetimes of 12 odd-parity levels of Ni II in the energy range from 51550 to 57080  $\text{cm}^{-1}$  are reported in that paper. Later, Fedchak & Lawler (1999) improved the experimental setup, confirmed and extended the previous results to a total of 18 experimental lifetimes and reported transition probabilities for 59 lines in the VUV and UV spectrum of  $\text{Ni}^+$ , Ni II.

In the present work, we have measured lifetimes for seven even-parity levels in the energy range 98400 to 100600  $\text{cm}^{-1}$ . The lifetimes are measured using the TR-LIF method, and the high-lying states are populated using two-step photon excitation of ions produced by laser ablation. Furthermore, we report theoretical lifetimes obtained with a pseudo-relativistic Hartree-Fock method in good agreement with the experimental results, and calculated transition probabilities for 477 lines depopulating highly excited levels belonging to the even-parity  $3d^84d$  configuration in singly ionized nickel.

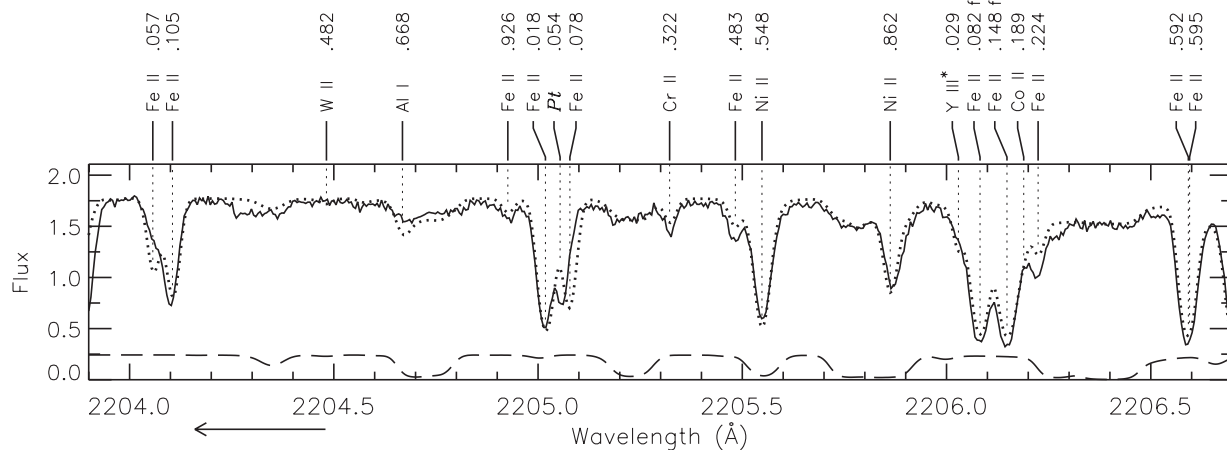


**Fig. 1.** The *HST*/GHRS spectrum of Chi Lupi in the region around 2205 Å, showing the prominent Ni II lines at 2205.548 and 2205.862 Å studied in the present work. The solid line is the observed spectrum and the dashed line is the synthetic spectrum. Courtesy of Brandt et al. (1999) and reproduced by permission of the AAS.

The lines studied in the present work appear strong in spectra of hot stars, such as the B9.5V type HgMn star Chi Lupi A (Brandt et al. 1999), where the lines form prominent absorption features despite their higher excitation. As an example, a spectral segment of Chi Lupi from the *HST*/GHRS atlas is presented in Figure 1. In addition, the Ni II lines are identified in several cooler template stars, e.g. the solar type star  $\alpha$  Cen A (spectral type G2 V) and Arcturus (K1.5 III) as reported by Hinkle et al. (2005). In the linelists of these stars, several Ni II lines are presented without multiplet number, indicating that they are of too high excitation to be listed in the multiplet table by Moore (1959). All the Ni II lines in the 2000-3000 Å region without multiplet number are included in our study.

## 2. Experiment

The ground term in Ni II is  $[\text{Ar}] 3d^9 2D$ , but as a starting point in the excitation schemes we used the  $J = 9/2$  and  $7/2$  levels in the second lowest term of even parity,  $3d^8(^3F)4s^4F$ , at 8394 and 9330  $\text{cm}^{-1}$ , respectively (Shenstone 1970). These levels were populated directly in the plasma produced by the ablation laser. The first tuneable laser excited the intermediate, odd parity, levels in the  $3d^84p$  configuration around 55000  $\text{cm}^{-1}$ , from where the final, even parity, levels in  $3d^84d$  around 100000  $\text{cm}^{-1}$  were reached with the second tuneable laser. The excitation and detection channels used in this work are given in Table 1.

The experimental set-up for two-step excitations at the Lund High Power Laser Facility has recently been described by Lundberg et al. (2016), and for an overview we refer to Figure 1 in that paper. Here we only give the most important details. Ni<sup>+</sup> ions in the  $3d^8(^3F)4s^4F$  term were created by focusing 532 nm, 10 ns long, laser pulses onto a rotating nickel target placed in a vacuum chamber with a pressure of about  $10^{-4}$  mbar. The two short wavelength excitation laser beams entered the vacuum chamber at a small relative angle and were focused on the expanding plasma plume about 5 mm above the target. All lasers operated at 10 Hz and were synchronized by a delay generator. The time resolved fluorescence from the excited states (both intermediate and final) was detected at right angles to the lasers by a 1/8 m grating monochromator, with its 0.28 mm wide entrance slit oriented parallel to the excitation laser beams and perpendicular to the ablation laser. The dispersed light was registered

by a fast micro-channel-plate photomultiplier tube (Hamamatsu R3809U) and digitized by a Tektronix DPO 7254 oscilloscope. A second channel on the oscilloscope simultaneously registered the excitation pulse shape, as detected by a fast photo diode. The PM tube has a rise time of 200 ps and the oscilloscope sampled the decay and pulse shape at every 50 ps. All spectral measurements were performed in the second spectral order, which is closer to the optimum efficiency of the blazed grating, resulting in a linewidth of about 0.5 nm.

For both the first and the second excitations we used the frequency tripled output from Nd:YAG pumped dye lasers (Continuum Nd-60), primarily operating with DCM dye. The first step had a pulse length of 10 ns whereas, by injection seeding and compressing, for the second Nd:YAG laser a pulse length of about 1 ns could be obtained. Before every measurement the delay between the two lasers was checked and, if necessary, adjusted so that the short pulse from second laser coincided with the maximum population of the intermediate level. The short pulse length in the second step and the high time resolution of the detection system is necessary to accurately measure the short lifetimes involved (1.2 - 1.3 ns). To reach a sufficient statistical accuracy each decay curve was averaged over 1000 laser pulses. The final lifetime analysis used the code DECFIT (Palmeri et al. 2008) to fit a single exponential decay, convoluted by the measured pulse shape, and a background function to the observed decay curve. Typically 10 to 20 measurements, performed during different days, were averaged to obtain the final lifetimes, given in Table 2. The quoted uncertainties in the results are mainly due to the scatter between the individual measurements.

As discussed by Lundberg et al. (2016), two step measurements may lead to complicated blending situations that must be taken into account in the planning and execution of the experiment. In the Ni case, we note from Table 1 that the two excitation lasers as well as the fluorescence channels all occur in the narrow wavelength interval 210 - 226 nm. Thus, most of the recorded decay curves are influenced by the very intense decay from the intermediate levels. This contribution extends over more than 10ns, due to the length of the first step laser pulses, and is noticeable even at rather large wavelength differences. Fortunately, this effect may be accurately compensated for by subtracting a separate decay measurement, with the second step laser blocked, before the final lifetime analysis. A worse case is encountered in

the measurement of the 4d<sup>4</sup>H<sub>13/2</sub> level where also scattered light from the second laser influences the decay. This is illustrated in Figure 2, and corrected for by a 'background' measurement where the second laser is not blocked but detuned slightly from resonance. Finally, transitions from levels in the 3d<sup>8</sup>4p configuration populated through the decay of the 4d level under investigation, so called cascades, may cause blending problems. Since this cannot be compensated for, one has to carefully choose the fluorescence channels to use, and if no sufficiently intense channels remain this particular level has to be omitted from the investigation. An example of this is the failure to measure the 4d<sup>4</sup>G<sub>7/2</sub> level at 100475.8 cm<sup>-1</sup> since all strong decay channels are blended by cascades.

### 3. Theoretical calculations

Calculations of energy levels and radiative transition rates in Ni II have been carried out using the relativistic Hartree-Fock (HFR) approach (Cowan 1981) modified to take core-polarization effects into account (Quinet et al. 1999, 2002). This method (HFR+CPOL) has been combined with a least-squares optimization process of the radial parameters to reduce the discrepancies between the Hamiltonian eigenvalues and the available experimental energy levels from Shenstone (1970). The following 23 configurations were explicitly introduced in the calculations: 3d<sup>9</sup>, 3d<sup>8</sup>4d, 3d<sup>8</sup>5d, 3d<sup>7</sup>4s4d, 3d<sup>7</sup>4s5d, 3d<sup>6</sup>4s<sup>2</sup>4d, 3d<sup>8</sup>4s, 3d<sup>8</sup>5s, 3d<sup>7</sup>4s<sup>2</sup>, 3d<sup>7</sup>4s5s, 3d<sup>6</sup>4s<sup>2</sup>5s for the even parity and 3d<sup>8</sup>4p, 3d<sup>8</sup>5p, 3d<sup>7</sup>4s4p, 3d<sup>7</sup>4s5p, 3d<sup>6</sup>4s<sup>2</sup>4p, 3d<sup>6</sup>4s<sup>2</sup>5p, 3d<sup>8</sup>4f, 3d<sup>8</sup>5f, 3d<sup>7</sup>4s4f, 3d<sup>7</sup>4s5f, 3d<sup>6</sup>4s<sup>2</sup>4f, 3d<sup>6</sup>4s<sup>2</sup>5f for the odd parity.

The ionic core considered for the core-polarization model potential and the correction to the transition dipole operator was a 3d<sup>6</sup> Ni V core. The dipole polarizability,  $\alpha_d$ , for such a core is 0.94 a<sub>0</sub><sup>3</sup> according to Fraga et al. (1976). We used the HFR mean radius of the outermost 3d core orbital, 1.004 a<sub>0</sub>, for the cut-off radius.

For the 3d<sup>9</sup>, 3d<sup>8</sup>4d, 3d<sup>8</sup>5d, 3d<sup>8</sup>4s, 3d<sup>8</sup>5s, 3d<sup>7</sup>4s<sup>2</sup> even configurations and the 3d<sup>8</sup>4p, 3d<sup>8</sup>5p, 3d<sup>7</sup>4s4p, 3d<sup>8</sup>4f, 3d<sup>8</sup>5f odd configurations, the average energies ( $E_{av}$ ), the electrostatic direct ( $F^k$ ) and exchange ( $G^k$ ) integrals, the spin-orbit ( $\zeta_{nl}$ ) and the effective interaction ( $\alpha$ ) parameters were allowed to vary during the fitting process. All other Slater integrals were scaled down by a factor 0.80 following a well-established procedure (Cowan 1981). The standard deviations of the fits were 212 cm<sup>-1</sup> for the even parity and 77 cm<sup>-1</sup> for the odd parity.

### 4. Results and discussion

The radiative lifetimes measured and computed in the present work are presented in Table 2. The theoretical lifetimes obtained in this work agree with the experimental values within about 5%. Table 2 includes the theoretical lifetimes obtained by Kurucz (2011). The latter work also used a semi-empirical approach based on a superposition of configurations calculation with a modified version of the Cowan codes (Cowan 1981) and experimental level energies (Shenstone 1970) to improve the results. In this case the calculated values are about 11% higher than the experiments.

Table 3 presents the computed oscillator strengths and transition probabilities for the strongest transitions (log  $gf > -4$ ) de-populating the even 3d<sup>8</sup>4d levels located in the range 98467–103664 cm<sup>-1</sup>. This table also presents the cancellation factors ( $CF$ ) as defined by Cowan (1981). Transitions with a  $CF$  lower than 0.05 should be considered with great care as they are affected by cancellation effects.

Most of the previous experimental and theoretical studies of radiative parameters in Ni II were focused on the spectral lines from the odd parity 3d<sup>8</sup>4p configuration (Zsargó & Federman 1998; Fedchak & Lawler 1999; Fritzsche et al. 2000; Fedchak et al. 2000; Jenkins & Tripp 2006; Manrique et al. 2011) and the 3d<sup>8</sup>4s - 3d<sup>8</sup>4p or 3d<sup>9</sup> - 3d<sup>8</sup>4p transitions. Recently, an extensive calculation of atomic structure data for Ni II was published by Cassidy et al. (2016). This work resulted in transition rates and oscillator strengths for 5023 electric dipole lines involving the 3d<sup>9</sup>, 3d<sup>8</sup>4s, 3d<sup>7</sup>4s<sup>2</sup>, 3d<sup>8</sup>4p and 3d<sup>7</sup>4s4p configurations.

To our knowledge, the only work listing also oscillator strengths from the 3d<sup>8</sup>4d even levels is the database of Kurucz (2011). Figure 3 shows a good general agreement between the two data sets. However, a closer inspection reveals that our new oscillator strengths are systematically higher than the values by Kurucz (2011). The mean ratio  $gf(\text{This work})/gf(\text{Kurucz})$  is 1.22 for lines with log  $gf > -4$ . The new log  $gf$  values are thus on average 20% larger than the previous calculation by Kurucz (2011). The difference between the two sets of results is possibly due to different values of the radial dipole integrals in calculations of the line strengths. In the case of 3d<sup>8</sup>4p - 3d<sup>8</sup>4d transition array for example, the reduced matrix element  $\langle 4p || r || 4d \rangle$  computed in our work was -4.55664 a.u. and -4.66532 a.u. with and without core-polarization, respectively, while, as far as we understand, Kurucz used a value scaled down to -4.47840 a.u. which tends to weaken the corresponding oscillator strengths.

### 5. Conclusion

We report seven new experimental radiative lifetimes for 3d<sup>8</sup>4d levels in Ni II, measured by two-step excitation using time-resolved laser-induced fluorescence on a laser ablation plasma. In addition, we report an extensive theoretical study using a relativistic Hartree-Fock technique optimized on experimental level energies. The theoretical and experimental lifetimes agree within 5%, which serves as benchmark for the accuracy of the 477 calculated oscillator strengths for the strong transitions around 200-220 nm belonging to the 3d<sup>8</sup>4p - 3d<sup>8</sup>4d transition array. Furthermore, on a two-standard deviation level the new theoretical  $gf$  values as well as the results from Kurucz (2011) agree with the experimental lifetimes.

*Acknowledgements.* This work has received funding from LASERLAB-EUROPE (grant agreement no. 284464, EC's Seventh Framework Programme), the Swedish Research Council through the Linnaeus grant to the Lund Laser Centre and a VR project grant 621-2011-4206 (H.H.), and the Knut and Alice Wallenberg Foundation. P.P. and P.Q. are respectively Research Associate and Research Director of the Belgian National Fund for Scientific Research F.R.S.-FNRS from which financial support is gratefully acknowledged. V.F. acknowledges the Belgian Scientific Policy (BELSPO) for her Return Grant. P.Q., V.F., P.P., G.M. and K.B. are grateful to the colleagues from Lund Laser Center for their kind hospitality and support.

### References

- Brandt, J. C., Heap, S. R., Beaver, E. A., et al. 1999, AJ, 117, 1505
- Cassidy, C. M., Hibbert, A., & Ramsbottom, C. A. 2016, A&A, 587, A107
- Cowan, R. D. 1981, The theory of atomic structure and spectra, (University of California Press, Berkeley)
- Engström, L., Lundberg, H., Nilsson, H., Hartman, H., & Bäckström, E. 2014, A&A, 570, A34
- Fedchak, J. A. & Lawler, J. E. 1999, ApJ, 523, 734
- Fedchak, J. A., Wiese, L. M., & Lawler, J. E. 2000, ApJ, 538, 773
- Fraga, S., Karwowski, J., & Saxena, K. 1976, Handbook of Atomic Data (Elsevier, Amsterdam)
- Fritzsche, S., Dong, C. Z., & Gaigalas, G. 2000, Atomic Data and Nuclear Data Tables, 76, 155

- Hartman, H., Nilsson, H., Engström, L., & Lundberg, H. 2015, A&A, 584, A24
- Hinkle, K., Wallace, L., Valenti, J., & Ayres, T. 2005, Ultraviolet Atlas of the Arcturus Spectrum, 1150-3800 Å. (San Francisco: ASP)
- Jenkins, E. B. & Tripp, T. M. 2006, ApJ, 637, 548
- Kurucz, R. 2011, <http://kurucz.harvard.edu>
- Lawler, J. E. & Salih, S. 1987, Phys. Rev. A, 35, 5046
- Lind, K., Bergemann, M., & Asplund, M. 2012, MNRAS, 427, 50
- Lundberg, H., Hartman, H., Engström, L., et al. 2016, MNRAS
- Manrique, J., Aguilera, J. A., & Aragón, C. 2011, J. Quant. Spectr. Rad. Transf., 112, 85
- Moore, C. E. 1959, A multiplet table of astrophysical interest. Part 1. (NBS Technical Note, Washington: US Department of Commerce)
- Nadyozhin, D. K. 2003, MNRAS, 346, 97
- Palmeri, P., Quinet, P., Fivet, V., et al. 2008, Phys. Scr, 78, 015304
- Quinet, P., Fivet, V., Palmeri, P., et al. 2016, MNRAS, in press
- Quinet, P., Palmeri, P., Biémont, E., et al. 2002, J. Alloys Comp., 344, 255
- Quinet, P., Palmeri, P., Biémont, E., et al. 1999, MNRAS, 307, 934
- Shenstone, A. 1970, J. Res. Natl. Bur. Stand., 76A, 801
- Stritzinger, M., Mazzali, P. A., Sollerman, J., & Benetti, S. 2006, A&A, 460, 793
- Wongwathanarat, A., Janka, H.-T., & Müller, E. 2011, in Proceedings of the International Astronomical Union, Vol. 7, Death of Massive Stars: Supernovae and Gamma-Ray Bursts, 150–153
- Zsargó, J. & Federman, S. R. 1998, ApJ, 498, 256

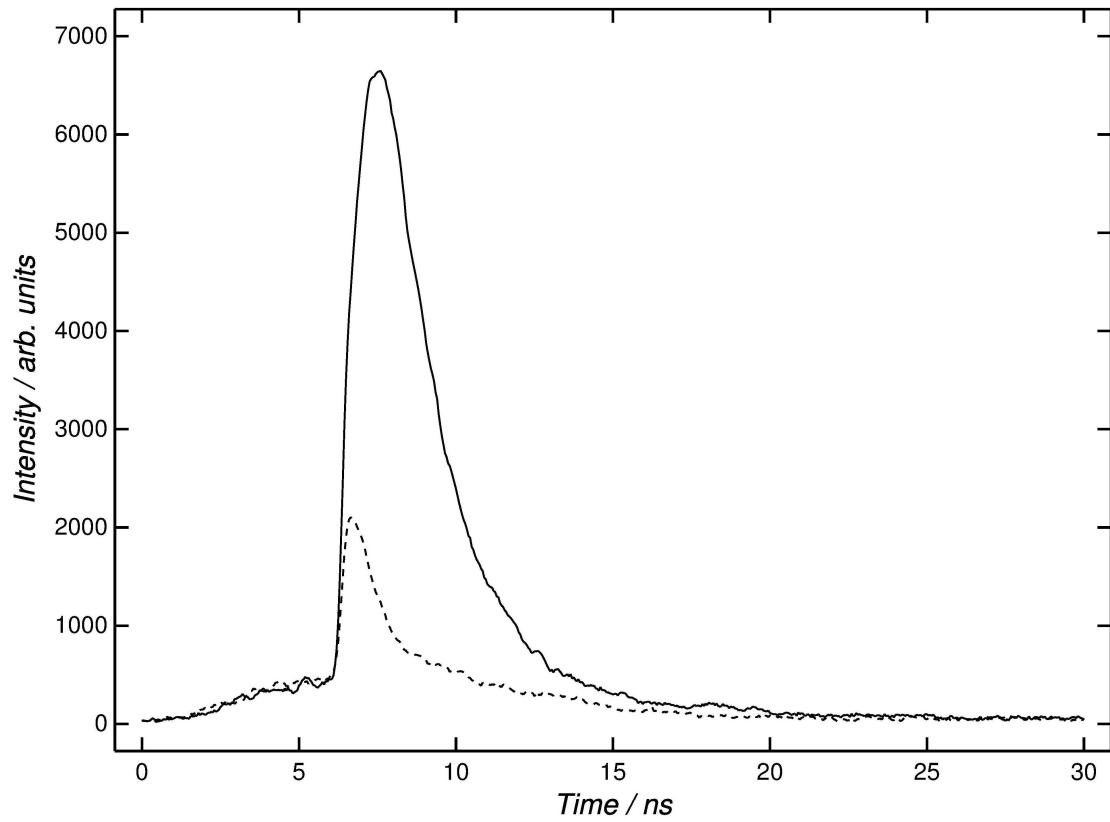


**Fig. 2.** The solid line shows the first 30 ns of the decay of  $4d\ 4H_{13/2}$  in Ni II. The dashed line shows the combined background contribution from both the first- and second-step lasers, where the latter is detuned 0.04 nm from resonance. This background is subtracted before the final lifetime analysis.

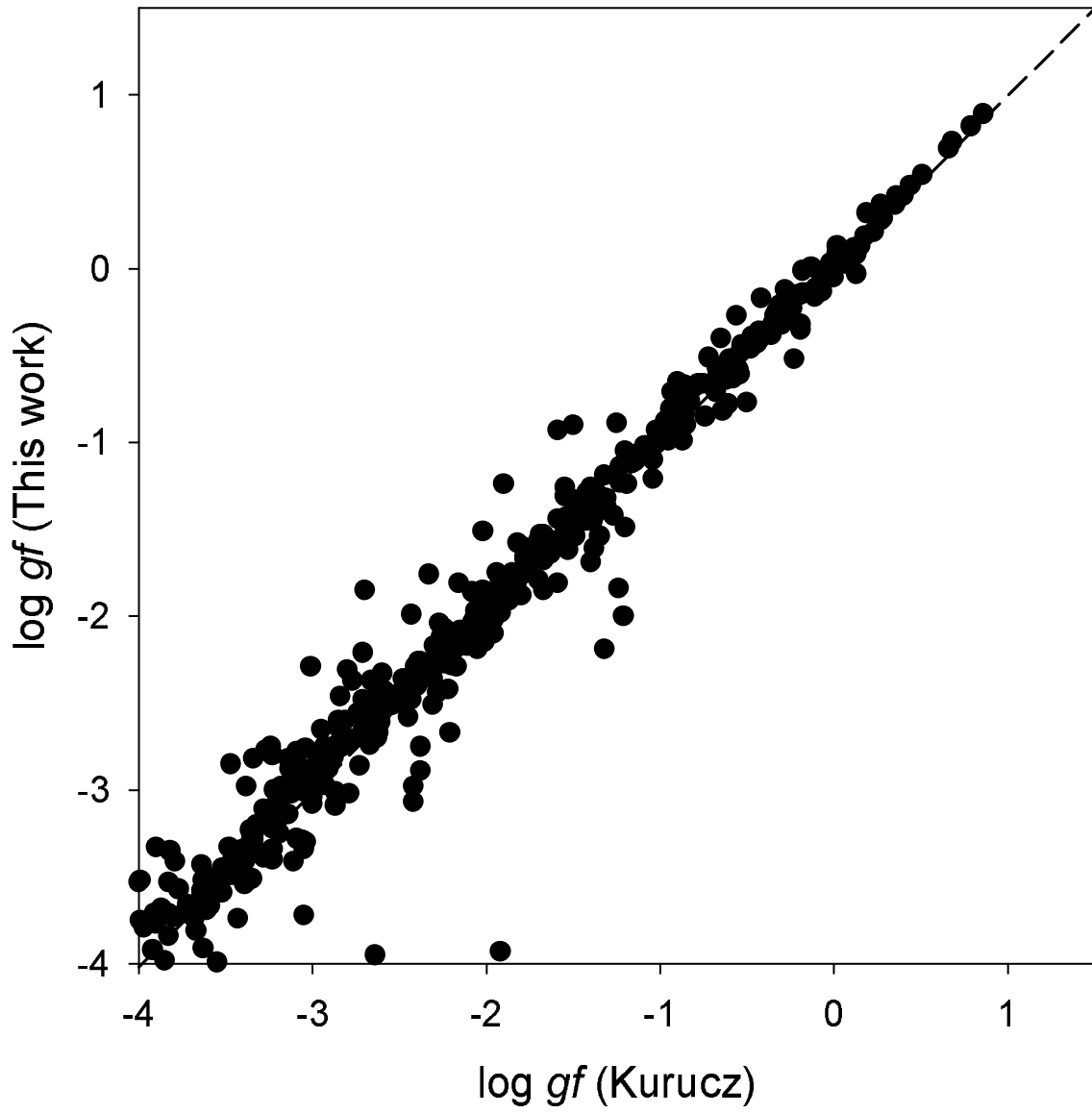


**Fig. 3.** Comparison between the oscillator strengths ( $\log gf$ ) calculated in the present work and those reported by Kurucz (2011) for transitions from highly excited even-parity  $3d^84d$  levels in Ni II.

**Table 1.** Levels measured in the  $3d^8(^3F)4d$  configuration of Ni II and the corresponding excitation schemes.

Final level	First step excitation <sup>a</sup>			Second step excitation			Detection	
	Start level $E^b(\text{cm}^{-1})$	Intermediate $E^b(\text{cm}^{-1})$	$\lambda_{air}$ (nm)	Final level $E^b(\text{cm}^{-1})$	$\lambda_{air}$ (nm)	Scheme <sup>c</sup>	Lower level $E^b(\text{cm}^{-1})$	$\lambda_{air}$ (nm)
$^4D_{7/2}$	8393.9	54557.0	216.6	98467.25	227.7	$3\omega + S$	51557.8	213 <sup>d</sup>
$^4H_{13/2}$	8393.9	53496.5	221.6	98822.55	220.6	$3\omega$	53496.5	221 <sup>e</sup>
$^4G_{11/2}$	8393.9	53496.5	221.6	99132.78	219.0	$3\omega$	54557.0	224 <sup>d</sup>
$^4F_{9/2}$	8393.9	53496.5	221.6	99154.81	218.9	$3\omega$	51557.8	210, 224 <sup>d</sup>
		54557.0	216.6		224.1	$3\omega + S$	54557.0	210
$^4D_{5/2}$	9330.0	55417.8	216.9	99559.33	226.5	$3\omega$	52738.4	214 <sup>d</sup>
$^4H_{11/2}$	9330.0	55299.6	217.5	100309.29	222.1	$3\omega$	55299.6	222 <sup>d</sup>
$^4G_{9/2}$	8393.9	54557.0	216.6	100619.26	217.0	$3\omega$	56371.4	226

<sup>a</sup> For all measured levels, the first excitation step used the frequency tripled ( $3\omega$ ) output from the dye laser

<sup>b</sup> Shenstone (1970)

<sup>c</sup> S imply one added Stokes component of  $4153\text{ cm}^{-1}$

<sup>d</sup> Corrected for fluorescence background from the intermediate level

<sup>e</sup> Corrected for scattered light from both lasers, see also Figure 2

**Table 2.** Radiative lifetimes (in ns) for selected energy levels belonging to the  $3d^8(^3F)4d$  configuration of Ni II.

Level	Energy <sup>a</sup> (cm <sup>-1</sup> )	Experiment	Calculations	
		This work	This work	Kurucz <sup>b</sup>
<sup>4</sup> D <sub>7/2</sub>	98467.25	1.28 ± 0.1	1.30	1.43
<sup>4</sup> H <sub>13/2</sub>	98822.55	1.25 ± 0.1	1.32	1.41
<sup>4</sup> G <sub>11/2</sub>	99132.78	1.32 ± 0.1	1.34	1.43
<sup>4</sup> F <sub>9/2</sub>	99154.81	1.20 ± 0.1	1.29	1.39
<sup>4</sup> D <sub>5/2</sub>	99559.33	1.37 ± 0.1	1.30	1.42
<sup>4</sup> H <sub>11/2</sub>	100309.29	1.30 ± 0.1	1.33	1.41
<sup>4</sup> G <sub>9/2</sub>	100619.26	1.25 ± 0.1	1.35	1.44

<sup>a</sup> Shenstone (1970)

<sup>b</sup> Kurucz (2011)



**Table 3.** Transition probabilities and oscillator strengths for spectral lines depopulating highly excited levels belonging to the even-parity 3d<sup>8</sup>4d configuration of Ni II.  $x\text{E}+y$  stands for  $x \times 10^y$ . Only transitions with  $\log gf \geq -4.0$  are listed in the table.

$\lambda^a$ (nm)	Lower odd level <sup>b</sup>		Upper 4d level <sup>b</sup>		HFR+CPOL <sup>c</sup>		
	$E$ (cm <sup>-1</sup> )	$J$	$E$ (cm <sup>-1</sup> )	$J$	$\log gf$	$gA$ (s <sup>-1</sup> )	$CF$
194.2965	51558	3.5	103026	2.5	-2.69	3.64E+06	0.018
196.3670	52738	2.5	103664	1.5	-3.74	3.12E+05	0.003
198.8580	52738	2.5	103026	2.5	-1.82	2.58E+07	0.077
199.2730	51558	3.5	101740	3.5	-3.04	1.54E+06	0.004
199.8845	53635	1.5	103664	1.5	-2.23	9.76E+06	0.100
200.7049	51558	3.5	101366	2.5	-3.20	1.04E+06	0.003
200.7409	51558	3.5	101357	4.5	-2.21	1.02E+07	0.054
201.1847	51558	3.5	101247	2.5	-3.36	7.19E+05	0.015
201.6016	51558	3.5	101145	3.5	-2.86	2.25E+06	0.009
202.0071	54176	0.5	103664	1.5	-2.96	1.80E+06	0.057
202.4010	53635	1.5	103026	2.5	-1.97	1.75E+07	0.237
203.7607	51558	3.5	100619	4.5	-0.93	1.90E+08	0.160
203.8699	51558	3.5	100593	3.5	-2.67	3.44E+06	0.002
204.0085	52738	2.5	101740	3.5	-1.19	1.03E+08	0.166
204.3583	51558	3.5	100476	3.5	-2.36	7.01E+06	0.020
204.7195	51558	3.5	100390	2.5	-1.91	1.96E+07	0.022
204.9606	51558	3.5	100332	4.5	-3.71	3.10E+05	0.004
205.5061	55019	2.5	103664	1.5	-2.47	5.32E+06	0.222
205.5783	52738	2.5	101366	2.5	-1.57	4.25E+07	0.031
206.0365	52738	2.5	101258	1.5	-2.17	1.06E+07	0.016
206.0817	52738	2.5	101247	2.5	-1.82	2.40E+07	0.082
206.5192	52738	2.5	101145	3.5	-1.53	4.61E+07	0.090
206.6519	53365	4.5	101740	3.5	-3.00	1.54E+06	0.003
208.2372	55019	2.5	103026	2.5	-3.28	8.07E+05	0.021
208.2606	51558	3.5	99559	2.5	-0.93	1.79E+08	0.041
208.3016	53365	4.5	101357	4.5	-3.84	2.20E+05	0.000
208.7672	51558	3.5	99443	4.5	-0.40	6.10E+08	0.347
208.9002	52738	2.5	100593	3.5	-0.25	8.54E+08	0.424
209.2143	51558	3.5	99341	3.5	-1.07	1.31E+08	0.252
209.2284	53365	4.5	101145	3.5	-3.53	4.45E+05	0.001
209.3466	52738	2.5	100491	1.5	-0.58	3.99E+08	0.116
209.4129	52738	2.5	100476	3.5	-0.90	1.89E+08	0.453
209.4386	53635	1.5	101366	2.5	-0.44	5.46E+08	0.354
209.7923	52738	2.5	100390	2.5	-2.29	7.72E+06	0.004
209.9142	53635	1.5	101258	1.5	-1.40	6.04E+07	0.045
209.9611	53635	1.5	101247	2.5	-1.02	1.43E+08	0.460
209.9665	53635	1.5	101246	0.5	-0.65	3.38E+08	0.605
209.9832	55418	3.5	103026	2.5	-1.45	5.42E+07	0.098
210.0308	51558	3.5	99155	4.5	-0.05	1.35E+09	0.675
210.0693	56075	2.5	103664	1.5	-2.28	7.95E+06	0.036
210.5587	54263	3.5	101740	3.5	-2.98	1.56E+06	0.001
211.1695	52738	2.5	100079	1.5	-0.17	1.01E+09	0.619
211.5549	53365	4.5	100619	4.5	-1.97	1.59E+07	0.004
211.6225	56424	1.5	103664	1.5	-1.52	4.55E+07	0.287
211.6727	53365	4.5	100593	3.5	-1.53	4.44E+07	0.045
211.7490	53635	1.5	100845	0.5	-1.84	2.17E+07	0.015
211.8727	54557	4.5	101740	3.5	-3.53	4.39E+05	0.001
212.1445	53496	5.5	100619	4.5	-2.80	2.33E+06	0.005
212.1991	53365	4.5	100476	3.5	-1.91	1.83E+07	0.030
212.2313	54263	3.5	101366	2.5	-1.60	3.74E+07	0.029
212.2716	54263	3.5	101357	4.5	-2.67	3.14E+06	0.001
212.3294	54176	0.5	101258	1.5	-0.14	1.06E+09	0.836
212.3829	54176	0.5	101246	0.5	-0.93	1.72E+08	0.381
212.6835	51558	3.5	98561	2.5	0.48	4.47E+09	0.859
212.7678	54263	3.5	101247	2.5	-1.36	6.45E+07	0.108
212.8486	53365	4.5	100332	4.5	-1.71	2.83E+07	0.013
212.9239	56075	2.5	103026	2.5	-1.90	1.85E+07	0.073

Table 3. continued.

$\lambda^a$ (nm)	Lower odd level <sup>b</sup>		Upper 4d level <sup>b</sup>		HFR+CPOL <sup>c</sup>		
	$E$ (cm <sup>-1</sup> )	$J$	$E$ (cm <sup>-1</sup> )	$J$	$\log gf$	$gA$ (s <sup>-1</sup> )	$CF$
212.9520	53365	4.5	100309	5.5	-1.21	9.12E+07	0.009
213.1096	51558	3.5	98467	3.5	0.41	3.78E+09	0.736
213.2342	54263	3.5	101145	3.5	-1.29	7.50E+07	0.024
213.3510	53635	1.5	100491	1.5	0.09	1.82E+09	0.775
213.5126	52738	2.5	99559	2.5	0.30	2.90E+09	0.744
213.5494	53496	5.5	100309	5.5	-1.86	2.02E+07	0.013
213.8139	53635	1.5	100390	2.5	-0.23	8.53E+08	0.708
213.9665	55019	2.5	101740	3.5	-1.12	1.10E+08	0.182
214.2068	54176	0.5	100845	0.5	-0.14	1.07E+09	0.852
214.2756	56371	3.5	103026	2.5	-1.64	3.34E+07	0.075
214.5150	52738	2.5	99341	3.5	-0.38	6.08E+08	0.617
214.5197	56424	1.5	103026	2.5	-2.15	1.02E+07	0.211
214.5819	54557	4.5	101145	3.5	-2.94	1.67E+06	0.011
215.2446	53635	1.5	100079	1.5	-0.78	2.40E+08	0.187
215.2610	55300	4.5	101740	3.5	-3.29	7.29E+05	0.001
215.5631	53635	1.5	100010	0.5	-0.14	1.04E+09	0.866
215.6511	54263	3.5	100619	4.5	-0.99	1.46E+08	0.038
215.6939	55019	2.5	101366	2.5	-0.61	3.51E+08	0.149
215.7734	54263	3.5	100593	3.5	-2.00	1.44E+07	0.007
215.8103	55418	3.5	101740	3.5	-1.81	2.21E+07	0.009
215.8464	54176	0.5	100491	1.5	-0.88	1.89E+08	0.238
215.9041	52738	2.5	99041	1.5	0.03	1.54E+09	0.868
216.1795	57420	2.5	103664	1.5	-0.49	4.60E+08	0.318
216.1983	55019	2.5	101258	1.5	-0.63	3.32E+08	0.435
216.2481	55019	2.5	101247	2.5	-0.18	9.38E+08	0.674
216.3205	54263	3.5	100476	3.5	0.10	1.78E+09	0.619
216.7253	54263	3.5	100390	2.5	-0.64	3.26E+08	0.291
216.7298	55019	2.5	101145	3.5	0.21	2.26E+09	0.369
216.9567	53365	4.5	99443	4.5	-0.52	4.32E+08	0.139
216.9955	54263	3.5	100332	4.5	0.41	3.60E+09	0.495
217.0296	54557	4.5	100619	4.5	-3.95	1.58E+05	0.000
217.0516	55300	4.5	101357	4.5	-1.45	5.07E+07	0.030
217.1535	54557	4.5	100593	3.5	-1.57	3.83E+07	0.043
217.4396	53365	4.5	99341	3.5	-0.32	6.76E+08	0.732
217.5677	55418	3.5	101366	2.5	-2.36	6.21E+06	0.005
217.5769	53496	5.5	99443	4.5	-0.89	1.81E+08	0.397
217.5832	57081	3.5	103026	2.5	-0.15	9.98E+08	0.540
217.6100	55418	3.5	101357	4.5	-0.87	1.92E+08	0.055
217.6795	53635	1.5	99559	2.5	-1.07	1.20E+08	0.076
217.7077	54557	4.5	100476	3.5	-2.10	1.13E+07	0.035
217.7847	54176	0.5	100079	1.5	-1.37	5.97E+07	0.095
218.1108	54176	0.5	100010	0.5	-1.54	4.02E+07	0.042
218.1316	55418	3.5	101247	2.5	-2.39	5.70E+06	0.010
218.1638	52738	2.5	98561	2.5	-1.62	3.36E+07	0.011
218.3217	53365	4.5	99155	4.5	0.37	3.25E+09	0.754
218.3913	54557	4.5	100332	4.5	-1.76	2.43E+07	0.045
218.4268	53365	4.5	99133	5.5	-0.35	6.22E+08	0.117
218.5002	54557	4.5	100309	5.5	-3.01	1.36E+06	0.000
218.6122	52738	2.5	98467	3.5	-1.02	1.34E+08	0.090
218.6217	55418	3.5	101145	3.5	-1.26	7.63E+07	0.035
218.9176	56075	2.5	101740	3.5	-0.69	2.83E+08	0.136
218.9497	53496	5.5	99155	4.5	-0.32	6.61E+08	0.876
219.0554	53496	5.5	99133	5.5	0.13	1.86E+09	0.732
219.2037	57420	2.5	103026	2.5	-0.21	8.65E+08	0.205
219.2092	53365	4.5	98969	5.5	0.73	7.40E+09	0.765
219.3535	55019	2.5	100593	3.5	-0.01	1.35E+09	0.770
219.8423	53496	5.5	98969	5.5	0.13	1.87E+09	0.918
219.8457	55019	2.5	100491	1.5	-1.05	1.23E+08	0.574
219.9189	55019	2.5	100476	3.5	0.01	1.40E+09	0.397
220.1659	53635	1.5	99041	1.5	-3.92	1.66E+05	0.000

Table 3. continued.

$\lambda^a$ (nm)	Lower odd level <sup>b</sup>		Upper 4d level <sup>b</sup>		HFR+CPOL <sup>c</sup>		
	$E$ (cm <sup>-1</sup> )	$J$	$E$ (cm <sup>-1</sup> )	$J$	$\log gf$	$gA$ (s <sup>-1</sup> )	$CF$
220.3373	55019	2.5	100390	2.5	-0.24	7.93E+08	0.559
220.3467	56371	3.5	101740	3.5	0.06	1.58E+09	0.551
220.5548	53496	5.5	98823	6.5	0.89	1.06E+10	0.928
220.5862	55300	4.5	100619	4.5	0.28	2.62E+09	0.710
220.6978	54263	3.5	99559	2.5	-0.36	6.06E+08	0.702
220.7142	55300	4.5	100593	3.5	-0.81	2.12E+08	0.283
220.7262	56075	2.5	101366	2.5	-0.21	8.43E+08	0.224
221.1630	55418	3.5	100619	4.5	-0.01	1.33E+09	0.245
221.2544	56075	2.5	101258	1.5	-2.19	8.86E+06	0.008
221.2668	54263	3.5	99443	4.5	0.08	1.65E+09	0.636
221.2867	55300	4.5	100476	3.5	-0.64	3.12E+08	0.587
221.2917	55418	3.5	100593	3.5	0.03	1.45E+09	0.423
221.3066	56075	2.5	101247	2.5	-1.32	6.60E+07	0.035
221.3155	58493	2.5	103664	1.5	-0.41	5.31E+08	0.319
221.6502	53365	4.5	98467	3.5	-0.46	4.68E+08	0.732
221.7690	54263	3.5	99341	3.5	-0.04	1.25E+09	0.589
221.8111	56075	2.5	101145	3.5	0.42	3.57E+09	0.943
221.8569	55019	2.5	100079	1.5	-1.11	1.04E+08	0.456
221.8671	55418	3.5	100476	3.5	-1.51	4.19E+07	0.016
221.9930	55300	4.5	100332	4.5	-0.71	2.66E+08	0.141
222.1055	55300	4.5	100309	5.5	0.82	8.89E+09	0.955
222.1791	56371	3.5	101366	2.5	-1.30	6.83E+07	0.257
222.2233	56371	3.5	101357	4.5	0.54	4.62E+09	0.640
222.2929	55418	3.5	100390	2.5	-1.58	3.61E+07	0.026
222.3629	58706	1.5	103664	1.5	0.09	1.67E+09	0.679
222.4415	56424	1.5	101366	2.5	0.19	2.11E+09	0.859
222.5161	53635	1.5	98561	2.5	-1.94	1.57E+07	0.017
222.5772	55418	3.5	100332	4.5	0.42	3.50E+09	0.950
222.6867	54263	3.5	99155	4.5	-0.27	7.25E+08	0.183
222.7183	54557	4.5	99443	4.5	0.32	2.84E+09	0.769
222.7672	56371	3.5	101247	2.5	-0.43	4.97E+08	0.858
222.8241	54176	0.5	99041	1.5	-2.29	6.93E+06	0.018
222.9781	56424	1.5	101258	1.5	0.06	1.56E+09	0.779
223.0310	56424	1.5	101247	2.5	-0.27	7.28E+08	0.429
223.0370	56424	1.5	101246	0.5	-1.69	2.75E+07	0.297
223.2272	54557	4.5	99341	3.5	-1.87	1.81E+07	0.033
223.2784	56371	3.5	101145	3.5	-1.31	6.48E+07	0.073
223.8459	57081	3.5	101740	3.5	-0.43	4.96E+08	0.235
224.1569	54557	4.5	99155	4.5	-0.03	1.25E+09	0.348
224.2677	54557	4.5	99133	5.5	0.69	6.47E+09	0.972
224.4445	55019	2.5	99559	2.5	-3.35	5.98E+05	0.001
224.4861	58493	2.5	103026	2.5	0.09	1.63E+09	0.685
224.5600	56075	2.5	100593	3.5	-0.77	2.23E+08	0.135
225.0494	56424	1.5	100845	0.5	-0.73	2.47E+08	0.672
225.0759	56075	2.5	100491	1.5	-0.68	2.74E+08	0.408
225.0926	54557	4.5	98969	5.5	-2.19	8.53E+06	0.002
225.1526	56075	2.5	100476	3.5	-0.36	5.72E+08	0.171
225.5525	55019	2.5	99341	3.5	-1.81	2.05E+07	0.028
225.5613	57420	2.5	101740	3.5	-0.71	2.54E+08	0.179
225.5638	58706	1.5	103026	2.5	-0.46	4.59E+08	0.695
225.5911	56075	2.5	100390	2.5	-0.06	1.14E+09	0.414
225.6709	54263	3.5	98561	2.5	-1.35	5.87E+07	0.151
225.7372	57081	3.5	101366	2.5	-1.68	2.74E+07	0.073
225.7828	57081	3.5	101357	4.5	0.29	2.54E+09	0.970
225.9297	56371	3.5	100619	4.5	0.12	1.71E+09	0.545
226.0640	56371	3.5	100593	3.5	-0.52	3.92E+08	0.350
226.1507	54263	3.5	98467	3.5	-1.75	2.33E+07	0.040
226.3443	57081	3.5	101247	2.5	-1.10	1.03E+08	0.168
226.4653	55300	4.5	99443	4.5	-3.52	3.97E+05	0.000
226.4741	55418	3.5	99559	2.5	-0.27	7.12E+08	0.428

Table 3. continued.

$\lambda^a$ (nm)	Lower odd level <sup>b</sup>		Upper 4d level <sup>b</sup>		HFR+CPOL <sup>c</sup>		
	$E$ (cm <sup>-1</sup> )	$J$	$E$ (cm <sup>-1</sup> )	$J$	$\log gf$	$gA$ (s <sup>-1</sup> )	$CF$
226.6646	56371	3.5	100476	3.5	-0.63	3.06E+08	0.274
226.8598	56424	1.5	100491	1.5	-2.82	1.97E+06	0.004
226.8721	57081	3.5	101145	3.5	-2.40	5.11E+06	0.008
226.9915	55300	4.5	99341	3.5	-1.97	1.40E+07	0.017
227.0733	55418	3.5	99443	4.5	-0.32	6.27E+08	0.215
227.0887	55019	2.5	99041	1.5	-2.15	9.02E+06	0.079
227.1090	56371	3.5	100390	2.5	-1.29	6.68E+07	0.141
227.1843	56075	2.5	100079	1.5	-0.61	3.17E+08	0.373
227.3832	56424	1.5	100390	2.5	-1.43	4.84E+07	0.031
227.4057	56371	3.5	100332	4.5	-3.93	1.52E+05	0.000
227.4818	57420	2.5	101366	2.5	-0.90	1.60E+08	0.541
227.6023	55418	3.5	99341	3.5	-0.03	1.20E+09	0.364
227.6672	54557	4.5	98467	3.5	0.09	1.59E+09	0.901
227.9529	55300	4.5	99155	4.5	-1.81	2.00E+07	0.006
228.0430	57420	2.5	101258	1.5	-3.58	3.37E+05	0.021
228.0675	55300	4.5	99133	5.5	-1.61	3.17E+07	0.007
228.0983	57420	2.5	101247	2.5	-0.12	9.78E+08	0.702
228.5689	55418	3.5	99155	4.5	-0.51	4.01E+08	0.079
228.6343	57420	2.5	101145	3.5	-2.21	7.89E+06	0.036
228.9207	55300	4.5	98969	5.5	-1.49	4.15E+07	0.005
229.0019	56424	1.5	100079	1.5	-1.66	2.80E+07	0.059
229.3625	56424	1.5	100010	0.5	-0.99	1.31E+08	0.255
229.5899	55019	2.5	98561	2.5	-2.71	2.50E+06	0.019
229.6099	57081	3.5	100619	4.5	0.04	1.37E+09	0.373
229.7486	57081	3.5	100593	3.5	-0.20	7.98E+08	0.486
230.0865	55019	2.5	98467	3.5	-3.33	5.96E+05	0.008
230.3689	57081	3.5	100476	3.5	-0.13	9.27E+08	0.437
230.8280	57081	3.5	100390	2.5	-1.29	6.46E+07	0.116
231.0611	56075	2.5	99341	3.5	-1.66	2.73E+07	0.015
231.1346	57081	3.5	100332	4.5	-0.69	2.56E+08	0.100
231.1585	58493	2.5	101740	3.5	0.37	2.88E+09	0.937
231.5560	57420	2.5	100593	3.5	-0.41	4.80E+08	0.666
231.5840	55300	4.5	98467	3.5	-1.37	5.36E+07	0.130
231.7140	55418	3.5	98561	2.5	-1.01	1.22E+08	0.136
231.7599	56424	1.5	99559	2.5	-2.56	3.43E+06	0.009
232.1011	56371	3.5	99443	4.5	-0.65	2.79E+08	0.136
232.1046	57420	2.5	100491	1.5	-0.82	1.86E+08	0.575
232.1862	57420	2.5	100476	3.5	-0.85	1.74E+08	0.211
232.2198	55418	3.5	98467	3.5	-1.40	4.92E+07	0.037
232.6525	57420	2.5	100390	2.5	-0.39	5.00E+08	0.647
232.6537	56371	3.5	99341	3.5	-0.76	2.13E+08	0.156
232.6735	56075	2.5	99041	1.5	-1.54	3.57E+07	0.073
233.1759	58493	2.5	101366	2.5	-0.96	1.34E+08	0.207
233.6639	56371	3.5	99155	4.5	-1.76	2.13E+07	0.022
233.7655	58493	2.5	101258	1.5	-3.41	4.75E+05	0.008
233.8237	58493	2.5	101247	2.5	-0.35	5.39E+08	0.250
234.3388	58706	1.5	101366	2.5	-0.84	1.75E+08	0.533
234.3474	57420	2.5	100079	1.5	-0.11	9.41E+08	0.948
234.3870	58493	2.5	101145	3.5	-1.85	1.69E+07	0.026
234.5804	56424	1.5	99041	1.5	-2.44	4.44E+06	0.019
234.9343	58706	1.5	101258	1.5	-1.58	3.16E+07	0.335
234.9931	58706	1.5	101247	2.5	-0.64	2.73E+08	0.259
234.9998	58706	1.5	101246	0.5	-0.16	8.32E+08	0.917
235.2999	56075	2.5	98561	2.5	-2.04	1.11E+07	0.022
235.3396	57081	3.5	99559	2.5	-2.27	6.45E+06	0.015
235.8215	56075	2.5	98467	3.5	-2.74	2.19E+06	0.008
235.9867	57081	3.5	99443	4.5	-0.18	7.82E+08	0.259
236.5581	57081	3.5	99341	3.5	-0.15	8.49E+08	0.251
236.9517	56371	3.5	98561	2.5	-2.31	5.79E+06	0.461
237.2348	58706	1.5	100845	0.5	-0.90	1.49E+08	0.420

Table 3. continued.

$\lambda^a$ (nm)	Lower odd level <sup>b</sup>		Upper 4d level <sup>b</sup>		HFR+CPOL <sup>c</sup>		
	$E$ (cm <sup>-1</sup> )	$J$	$E$ (cm <sup>-1</sup> )	$J$	$\log gf$	$gA$ (s <sup>-1</sup> )	$CF$
237.2365	57420	2.5	99559	2.5	-1.38	4.95E+07	0.130
237.2502	56424	1.5	98561	2.5	-3.15	8.43E+05	0.010
237.4585	58493	2.5	100593	3.5	-1.14	8.48E+07	0.073
237.4807	56371	3.5	98467	3.5	-2.16	8.18E+06	0.168
237.6025	57081	3.5	99155	4.5	-1.24	6.81E+07	0.037
238.0354	58493	2.5	100491	1.5	-1.42	4.45E+07	0.214
238.1212	58493	2.5	100476	3.5	-0.66	2.55E+08	0.256
238.4747	57420	2.5	99341	3.5	-0.26	6.41E+08	0.430
238.6117	58493	2.5	100390	2.5	-0.80	1.85E+08	0.118
239.2474	58706	1.5	100491	1.5	-2.89	1.51E+06	0.008
239.8296	58706	1.5	100390	2.5	-0.57	3.08E+08	0.426
240.1926	57420	2.5	99041	1.5	-0.12	8.73E+08	0.653
240.3949	58493	2.5	100079	1.5	-0.95	1.29E+08	0.288
241.0028	57081	3.5	98561	2.5	-1.63	2.70E+07	0.268
241.5501	57081	3.5	98467	3.5	-1.63	2.68E+07	0.100
241.6311	58706	1.5	100079	1.5	-1.23	6.68E+07	0.297
242.0325	58706	1.5	100010	0.5	-0.67	2.44E+08	0.626
242.9924	57420	2.5	98561	2.5	-3.12	8.66E+05	0.021
243.4359	58493	2.5	99559	2.5	-3.33	5.33E+05	0.001
243.5488	57420	2.5	98467	3.5	-2.29	5.78E+06	0.097
244.7036	58706	1.5	99559	2.5	-2.07	9.57E+06	0.071
244.7398	58493	2.5	99341	3.5	-1.07	9.53E+07	0.063
246.5495	58493	2.5	99041	1.5	-0.66	2.42E+08	0.418
247.8500	58706	1.5	99041	1.5	-1.33	5.07E+07	0.147
250.0870	58493	2.5	98467	3.5	-2.75	1.91E+06	0.036
269.5188	66571	2.5	103664	1.5	-3.65	2.05E+05	0.005
269.5796	66580	1.5	103664	1.5	-2.51	2.83E+06	0.025
272.9010	67031	0.5	103664	1.5	-2.86	1.25E+06	0.077
274.2354	66571	2.5	103026	2.5	-2.27	4.75E+06	0.040
274.2984	66580	1.5	103026	2.5	-2.13	6.59E+06	0.120
277.9362	67695	2.5	103664	1.5	-2.19	5.63E+06	0.080
281.5343	68154	1.5	103664	1.5	-1.64	1.91E+07	0.060
282.5474	68282	0.5	103664	1.5	-2.28	4.42E+06	0.081
282.9548	67695	2.5	103026	2.5	-2.48	2.76E+06	0.055
286.2231	68736	2.5	103664	1.5	-3.57	2.19E+05	0.003
286.4951	68131	3.5	103026	2.5	-1.94	9.48E+06	0.227
286.6848	68154	1.5	103026	2.5	-2.04	7.41E+06	0.081
287.3149	66571	2.5	101366	2.5	-3.36	3.55E+05	0.013
288.1178	68966	1.5	103664	1.5	-1.90	1.01E+07	0.096
288.2991	66571	2.5	101247	2.5	-2.44	2.93E+06	0.074
288.3687	66580	1.5	101247	2.5	-2.60	2.00E+06	0.056
288.3788	66580	1.5	101246	0.5	-2.10	6.30E+06	0.250
289.1558	66571	2.5	101145	3.5	-3.68	1.66E+05	0.012
291.5482	68736	2.5	103026	2.5	-2.28	4.08E+06	0.020
291.7516	66580	1.5	100845	0.5	-2.37	3.32E+06	0.213
292.0816	67031	0.5	101258	1.5	-3.25	4.43E+05	0.145
292.1827	67031	0.5	101246	0.5	-3.77	1.31E+05	0.070
293.5143	68966	1.5	103026	2.5	-2.26	4.27E+06	0.062
293.6376	67695	2.5	101740	3.5	-2.04	7.09E+06	0.183
293.8446	66571	2.5	100593	3.5	-4.00	7.73E+04	0.003
294.8601	66571	2.5	100476	3.5	-2.51	2.34E+06	0.107
295.6126	66571	2.5	100390	2.5	-2.82	1.15E+06	0.049
295.6457	67031	0.5	100845	0.5	-3.92	9.29E+04	0.022
295.6857	66580	1.5	100390	2.5	-2.08	6.30E+06	0.330
296.9004	67695	2.5	101366	2.5	-2.82	1.16E+06	0.038
297.4520	68131	3.5	101740	3.5	-3.69	1.52E+05	0.004
297.9514	67695	2.5	101247	2.5	-2.12	5.68E+06	0.128
298.3541	66571	2.5	100079	1.5	-1.98	7.77E+06	0.297
298.7778	67031	0.5	100491	1.5	-3.04	6.86E+05	0.156
298.8666	67695	2.5	101145	3.5	-3.25	4.17E+05	0.006

Table 3. continued.

$\lambda^a$ (nm)	Lower odd level <sup>b</sup>		Upper 4d level <sup>b</sup>		HFR+CPOL <sup>c</sup>		
	$E$ (cm <sup>-1</sup> )	$J$	$E$ (cm <sup>-1</sup> )	$J$	$\log gf$	$gA$ (s <sup>-1</sup> )	$CF$
299.0412	66580	1.5	100010	0.5	-2.48	2.46E+06	0.213
300.8815	68131	3.5	101357	4.5	-3.10	5.90E+05	0.007
301.0098	68154	1.5	101366	2.5	-2.66	1.61E+06	0.035
302.0902	68154	1.5	101247	2.5	-1.72	1.39E+07	0.148
302.1012	68154	1.5	101246	0.5	-1.44	2.63E+07	0.534
302.5043	67031	0.5	100079	1.5	-3.19	4.67E+05	0.191
302.6849	70635	2.5	103664	1.5	-3.16	5.07E+05	0.042
302.9027	68736	2.5	101740	3.5	-2.19	4.67E+06	0.096
303.0524	66571	2.5	99559	2.5	-2.74	1.34E+06	0.037
303.1293	66580	1.5	99559	2.5	-2.70	1.47E+06	0.093
303.1336	67031	0.5	100010	0.5	-3.14	5.32E+05	0.187
303.3399	70707	1.5	103664	1.5	-3.22	4.44E+05	0.038
303.8783	67695	2.5	100593	3.5	-2.76	1.27E+06	0.033
304.8237	67695	2.5	100491	1.5	-3.68	1.50E+05	0.016
305.0758	66571	2.5	99341	3.5	-1.87	9.75E+06	0.338
305.7694	67695	2.5	100390	2.5	-2.60	1.80E+06	0.077
305.8047	68154	1.5	100845	0.5	-1.99	7.23E+06	0.268
306.3759	68736	2.5	101366	2.5	-3.27	3.79E+05	0.010
307.0003	68282	0.5	100845	0.5	-3.54	2.04E+05	0.024
307.4952	68736	2.5	101247	2.5	-2.67	1.50E+06	0.026
307.7161	68131	3.5	100619	4.5	-2.26	3.91E+06	0.132
307.8927	66571	2.5	99041	1.5	-1.66	1.54E+07	0.486
307.9652	68131	3.5	100593	3.5	-2.60	1.75E+06	0.078
307.9721	66580	1.5	99041	1.5	-2.65	1.56E+06	0.120
308.4700	68736	2.5	101145	3.5	-3.41	2.68E+05	0.014
308.5477	68966	1.5	101366	2.5	-3.45	2.50E+05	0.009
308.7035	67695	2.5	100079	1.5	-3.91	8.49E+04	0.012
309.0808	68131	3.5	100476	3.5	-2.48	2.29E+06	0.165
309.1570	68154	1.5	100491	1.5	-3.82	1.06E+05	0.006
309.6829	68966	1.5	101247	2.5	-2.29	3.59E+06	0.119
309.6946	68966	1.5	101246	0.5	-2.35	3.07E+06	0.202
309.9077	68131	3.5	100390	2.5	-3.71	1.35E+05	0.015
310.0120	70778	3.5	103026	2.5	-2.73	1.30E+06	0.089
310.1298	68154	1.5	100390	2.5	-1.88	9.15E+06	0.207
310.4604	68131	3.5	100332	4.5	-2.85	9.72E+05	0.037
312.3145	67031	0.5	99041	1.5	-3.29	3.48E+05	0.161
312.5083	66571	2.5	98561	2.5	-3.40	2.75E+05	0.020
312.5900	66580	1.5	98561	2.5	-2.92	8.34E+05	0.183
313.1486	68154	1.5	100079	1.5	-2.16	4.69E+06	0.273
313.4290	66571	2.5	98467	3.5	-2.02	6.46E+06	0.433
313.4608	71771	2.5	103664	1.5	-2.58	1.77E+06	0.171
313.5878	68966	1.5	100845	0.5	-2.75	1.21E+06	0.080
313.7361	67695	2.5	99559	2.5	-2.29	3.50E+06	0.249
313.8118	68736	2.5	100593	3.5	-2.45	2.38E+06	0.129
313.8231	68154	1.5	100010	0.5	-1.85	9.65E+06	0.415
314.4024	68282	0.5	100079	1.5	-3.52	2.05E+05	0.065
314.8202	68736	2.5	100491	1.5	-2.42	2.53E+06	0.148
314.9702	68736	2.5	100476	3.5	-1.80	1.06E+07	0.355
315.0823	68282	0.5	100010	0.5	-3.66	1.48E+05	0.035
315.8290	68736	2.5	100390	2.5	-3.52	1.99E+05	0.011
315.9051	67695	2.5	99341	3.5	-2.79	1.08E+06	0.060
318.0944	68131	3.5	99559	2.5	-2.48	2.22E+06	0.099
318.1374	68966	1.5	100390	2.5	-2.43	2.47E+06	0.220
318.3284	68154	1.5	99559	2.5	-2.88	8.74E+05	0.055
318.9266	67695	2.5	99041	1.5	-2.35	2.93E+06	0.290
318.9603	68736	2.5	100079	1.5	-1.54	1.85E+07	0.617
319.2776	68131	3.5	99443	4.5	-2.77	1.11E+06	0.032
319.5182	72375	1.5	103664	1.5	-1.67	1.40E+07	0.533
319.8589	71771	2.5	103026	2.5	-1.51	2.02E+07	0.581
320.3243	68131	3.5	99341	3.5	-2.37	2.78E+06	0.183

Table 3. continued.

$\lambda^a$ (nm)	Lower odd level <sup>b</sup>		Upper 4d level <sup>b</sup>		HFR+CPOL <sup>c</sup>		
	$E$ (cm <sup>-1</sup> )	$J$	$E$ (cm <sup>-1</sup> )	$J$	$\log gf$	$gA$ (s <sup>-1</sup> )	$CF$
321.3149	68966	1.5	100079	1.5	-3.15	4.62E+05	0.056
321.4008	70635	2.5	101740	3.5	-3.74	1.18E+05	0.006
322.0250	68966	1.5	100010	0.5	-2.78	1.07E+06	0.128
322.2422	68131	3.5	99155	4.5	-2.57	1.73E+06	0.077
323.6733	68154	1.5	99041	1.5	-2.61	1.55E+06	0.066
324.3358	68736	2.5	99559	2.5	-3.02	6.05E+05	0.024
325.8741	72986	1.5	103664	1.5	-2.84	9.27E+05	0.028
326.0705	70707	1.5	101366	2.5	-2.17	4.25E+06	0.129
326.1685	72375	1.5	103026	2.5	-2.82	9.55E+05	0.062
326.5761	70635	2.5	101247	2.5	-3.52	1.88E+05	0.019
326.6544	68736	2.5	99341	3.5	-1.67	1.33E+07	0.399
327.2246	70707	1.5	101258	1.5	-3.11	4.83E+05	0.021
327.3386	70707	1.5	101247	2.5	-2.70	1.25E+06	0.154
327.3516	70707	1.5	101246	0.5	-1.87	8.33E+06	0.764
327.6744	70749	0.5	101258	1.5	-2.12	4.76E+06	0.154
327.6759	70635	2.5	101145	3.5	-2.95	6.99E+05	0.056
327.8017	70749	0.5	101246	0.5	-2.31	3.06E+06	0.407
328.5283	68131	3.5	98561	2.5	-1.87	8.37E+06	0.517
328.7779	68154	1.5	98561	2.5	-3.87	8.27E+04	0.036
329.5460	68131	3.5	98467	3.5	-2.14	4.45E+06	0.249
329.8861	68736	2.5	99041	1.5	-1.44	2.22E+07	0.605
331.7045	70707	1.5	100845	0.5	-3.07	5.14E+05	0.022
332.1667	70749	0.5	100845	0.5	-1.62	1.47E+07	0.721
332.4053	68966	1.5	99041	1.5	-2.98	6.32E+05	0.060
332.7945	72986	1.5	103026	2.5	-1.26	3.38E+07	0.710
333.5773	71771	2.5	101740	3.5	-3.50	1.89E+05	0.029
333.7100	70635	2.5	100593	3.5	-2.05	5.33E+06	0.124
334.8505	70635	2.5	100491	1.5	-1.79	9.63E+06	0.233
335.0203	70635	2.5	100476	3.5	-3.09	4.86E+05	0.077
335.1901	68736	2.5	98561	2.5	-3.67	1.28E+05	0.028
335.3068	70778	3.5	100593	3.5	-3.34	2.75E+05	0.013
335.6522	70707	1.5	100491	1.5	-1.45	2.12E+07	0.583
335.9221	73903	0.5	103664	1.5	-1.57	1.60E+07	0.586
335.9920	70635	2.5	100390	2.5	-2.15	4.22E+06	0.178
336.1255	70749	0.5	100491	1.5	-2.20	3.71E+06	0.248
336.7992	70707	1.5	100390	2.5	-2.51	1.84E+06	0.084
337.6108	70778	3.5	100390	2.5	-3.69	1.19E+05	0.013
338.2669	70778	3.5	100332	4.5	-3.20	3.67E+05	0.096
339.1555	71771	2.5	101247	2.5	-3.41	2.23E+05	0.033
339.5382	70635	2.5	100079	1.5	-1.75	1.02E+07	0.573
340.2680	74283	0.5	103664	1.5	-2.50	1.80E+06	0.445
340.3625	70707	1.5	100079	1.5	-2.75	1.03E+06	0.053
340.4719	74301	1.5	103664	1.5	-3.68	1.23E+05	0.055
340.8491	70749	0.5	100079	1.5	-2.86	7.98E+05	0.068
341.1595	70707	1.5	100010	0.5	-1.88	7.59E+06	0.440
341.6483	70749	0.5	100010	0.5	-3.51	1.77E+05	0.011
345.6362	70635	2.5	99559	2.5	-1.45	2.02E+07	0.414
346.2577	72375	1.5	101247	2.5	-3.43	2.03E+05	0.027
346.4905	70707	1.5	99559	2.5	-2.25	3.17E+06	0.115
347.3494	70778	3.5	99559	2.5	-2.02	5.26E+06	0.125
348.0334	74301	1.5	103026	2.5	-2.64	1.27E+06	0.415
348.0883	71771	2.5	100491	1.5	-2.58	1.44E+06	0.209
348.2706	70635	2.5	99341	3.5	-3.72	1.06E+05	0.006
348.7608	70778	3.5	99443	4.5	-2.13	4.08E+06	0.122
349.3220	71771	2.5	100390	2.5	-3.39	2.21E+05	0.038
350.0101	70778	3.5	99341	3.5	-2.75	9.61E+05	0.116
351.9465	70635	2.5	99041	1.5	-1.85	7.70E+06	0.373
352.2540	72986	1.5	101366	2.5	-3.75	9.65E+04	0.020
352.3012	70778	3.5	99155	4.5	-2.98	5.71E+05	0.021
353.1567	71771	2.5	100079	1.5	-2.45	1.87E+06	0.260

Table 3. continued.

$\lambda^a$ (nm)	Lower odd level <sup>b</sup>		Upper 4d level <sup>b</sup>		HFR+CPOL <sup>c</sup>		
	$E$ (cm <sup>-1</sup> )	$J$	$E$ (cm <sup>-1</sup> )	$J$	$\log gf$	$gA$ (s <sup>-1</sup> )	$CF$
353.3552	70749	0.5	99041	1.5	-3.98	5.59E+04	0.009
353.7344	72986	1.5	101247	2.5	-2.88	7.13E+05	0.079
353.7495	72986	1.5	101246	0.5	-3.08	4.44E+05	0.073
355.5737	72375	1.5	100491	1.5	-3.92	6.29E+04	0.026
356.8612	72375	1.5	100390	2.5	-2.97	5.60E+05	0.143
358.9066	70707	1.5	98561	2.5	-3.61	1.28E+05	0.010
359.1988	70635	2.5	98467	3.5	-2.61	1.29E+06	0.067
359.7584	71771	2.5	99559	2.5	-2.97	5.57E+05	0.065
359.8284	70778	3.5	98561	2.5	-1.24	3.01E+07	0.685
361.0496	70778	3.5	98467	3.5	-1.40	2.07E+07	0.446
361.7601	72375	1.5	100010	0.5	-3.40	2.04E+05	0.149
362.6134	71771	2.5	99341	3.5	-3.35	2.26E+05	0.022
363.4627	72986	1.5	100491	1.5	-3.73	9.59E+04	0.019
364.8080	72986	1.5	100390	2.5	-3.71	9.78E+04	0.026
366.6000	71771	2.5	99041	1.5	-3.99	5.08E+04	0.006
366.7136	76402	2.5	103664	1.5	-2.65	1.12E+06	0.020
368.7905	75918	3.5	103026	2.5	-2.33	2.30E+06	0.037
370.7754	74283	0.5	101246	0.5	-3.34	2.16E+05	0.216
374.4756	71771	2.5	98467	3.5	-3.45	1.68E+05	0.065
374.9122	72375	1.5	99041	1.5	-3.79	7.70E+04	0.041
375.5006	76402	2.5	103026	2.5	-3.01	4.68E+05	0.023
376.0069	73903	0.5	100491	1.5	-3.45	1.68E+05	0.101
376.2053	72986	1.5	99559	2.5	-3.12	3.60E+05	0.080
376.3696	74283	0.5	100845	0.5	-3.97	4.95E+04	0.062
381.4587	75149	4.5	101357	4.5	-3.79	7.50E+04	0.100
381.9278	73903	0.5	100079	1.5	-3.81	7.14E+04	0.072
387.1473	75918	3.5	101740	3.5	-3.38	1.82E+05	0.025
387.5554	74283	0.5	100079	1.5	-3.49	1.41E+05	0.197
388.5890	74283	0.5	100010	0.5	-3.86	6.01E+04	0.157
392.9771	75918	3.5	101357	4.5	-2.62	1.04E+06	0.151
394.5487	76402	2.5	101740	3.5	-1.57	1.15E+07	0.545
394.6811	75918	3.5	101247	2.5	-3.49	1.38E+05	0.026
397.6995	73903	0.5	99041	1.5	-3.29	2.20E+05	0.182
400.4618	76402	2.5	101366	2.5	-2.81	6.39E+05	0.234
402.3762	76402	2.5	101247	2.5	-1.75	7.35E+06	0.543
403.8052	74283	0.5	99041	1.5	-3.57	1.06E+05	0.131
404.0471	76402	2.5	101145	3.5	-2.48	1.34E+06	0.294
404.7172	75918	3.5	100619	4.5	-1.95	4.53E+06	0.474
405.1483	75918	3.5	100593	3.5	-2.36	1.76E+06	0.357
407.0812	75918	3.5	100476	3.5	-1.95	4.51E+06	0.596
408.5168	75918	3.5	100390	2.5	-3.50	1.28E+05	0.060
409.4777	75918	3.5	100332	4.5	-2.17	2.66E+06	0.462
413.2612	76402	2.5	100593	3.5	-2.35	1.75E+06	0.229
415.2724	76402	2.5	100476	3.5	-2.88	5.04E+05	0.168
416.7665	76402	2.5	100390	2.5	-1.92	4.61E+06	0.559
424.9559	75918	3.5	99443	4.5	-1.83	5.43E+06	0.394
426.8121	75918	3.5	99341	3.5	-1.65	8.29E+06	0.667
430.0280	75722	5.5	98969	5.5	-3.96	4.00E+04	0.044
430.2238	75918	3.5	99155	4.5	-2.46	1.26E+06	0.237
431.7079	76402	2.5	99559	2.5	-3.01	3.55E+05	0.145
435.8254	76402	2.5	99341	3.5	-3.23	2.07E+05	0.030
443.3420	75918	3.5	98467	3.5	-3.84	4.90E+04	0.015
456.1340	79823	3.5	101740	3.5	-3.02	3.04E+05	0.299
468.8767	79823	3.5	101145	3.5	-3.84	4.35E+04	0.185
481.3303	79823	3.5	100593	3.5	-3.51	8.85E+04	0.188
483.0646	79924	4.5	100619	4.5	-3.34	1.32E+05	0.165
489.8621	79924	4.5	100332	4.5	-3.59	7.05E+04	0.263
512.1791	79924	4.5	99443	4.5	-3.30	1.29E+05	0.095
512.2174	79823	3.5	99341	3.5	-3.47	8.73E+04	0.062
519.8509	79924	4.5	99155	4.5	-3.67	5.31E+04	0.038



<sup>a</sup> Vacuum ( $\lambda < 200$  nm) and air ( $\lambda > 200$  nm) Ritz wavelengths deduced from the experimental energy level values by Shenstone (1970)

<sup>b</sup> Energies from Shenstone (1970). Energy values have been rounded to the nearest unit.

<sup>c</sup> This work.